Research Square

Preprints are preliminary reports that have not undergone peer review.
They should not be considered conclusive, used to inform clinical practice,
or referenced by the media as validated information.

CIP2A promotes osteoclastogenesis and postmenopausal bone loss by activating a novel HMGA1–c-Myc–PI3K/AKT axis

Meipeng Zhu
Huazhong University of Science and Technology Tongji Medical College Tongji Hospital
Jinpeng He
Huazhong University of Science and Technology Tongji Medical College Tongji Hospital
Junhong Li
Huazhong University of Science and Technology Tongji Medical College Tongji Hospital
Honglei Kang
Huazhong University of Science and Technology Tongji Medical College Tongji Hospital
Yimin Dong
Huazhong University of Science and Technology Tongji Medical College Tongji Hospital
Shiheng Wang
Huazhong University of Science and Technology Tongji Medical College Tongji Hospital
Yan Mou
Wuhan Red Cross Hospital
Yayun Zhang
Huazhong University of Science and Technology Tongji Medical College Tongji Hospital
Jian Liu
Huazhong University of Science and Technology Tongji Medical College Tongji Hospital
Xuying Sun
Huazhong University of Science and Technology Tongji Medical College Tongji Hospital
Feng Li
lifengmd@hust.edu.cn

Huazhong University of Science and Technology Tongji Medical College Tongji Hospital

Research Article

Keywords: Osteoporosis, CIP2A, Osteoclast, HMGA1, c-Myc, Deubiquitination, PI3K/AKT signaling

Posted Date: August 20th, 2026

DOI: https://doi.org/10.21203/rs.3.rs-9848947/v1

License: This work is licensed under a Creative Commons Attribution 4.0 International License.
Read Full License

Abstract

Background

Osteoclast-mediated bone resorption drives osteoporosis, a prevalent skeletal disorder with significant clinical and socioeconomic burden, yet the upstream molecular mechanisms controlling osteoclast differentiation remain incompletely defined. Cancerous inhibitor of protein phosphatase 2A (CIP2A) is a known oncogenic regulator, but its role in bone metabolism and osteoclast biology has not been explored.

Methods

We used RANKL-induced mouse bone marrow macrophages (BMMs) to model osteoclast differentiation in vitro, with adenoviral-mediated gain- or loss-of-function of CIP2A. Mechanistic investigations included immunoprecipitation-mass spectrometry (IP-MS), co-immunoprecipitation (co-IP), ubiquitination assays, cycloheximide (CHX) chase analysis, RNA sequencing (RNA-seq), and chromatin immunoprecipitation sequencing (ChIP-seq). For translational assessment, in vivo, we employed an ovariectomy (OVX)-induced osteoporosis mouse model with systemic adeno-associated virus (AAV)-mediated gene manipulation as well as pharmacological inhibition using the CIP2A small-molecule inhibitor TD52.

Results

CIP2A expression was dynamically upregulated during RANKL-induced osteoclastogenesis. CIP2A promoted osteoclast formation, actin ring assembly, and bone resorptive activity in vitro, without affecting osteoblast differentiation. Mechanistically, CIP2A acted as a molecular scaffold that recruited the deubiquitinase OTUD4 to stabilize high mobility group A1 (HMGA1) by preventing its ubiquitination and proteasomal degradation. Stabilized HMGA1 translocated to the nucleus. Integrated multi-omics analyses (RNA-seq and HMGA1 ChIP-seq) identified c-Myc as a direct transcriptional target of HMGA1, which bound distal regulatory elements to enhance c-Myc transcription. Functional experiments further revealed that c-Myc formed a positive feedback loop with the phosphatidylinositol 3-kinase/protein kinase B (PI3K/AKT) pathway, sustaining osteoclast activity. In OVX mice, c-Myc overexpression or AKT activation partially rescued the bone loss induced by CIP2A knockdown. Importantly, pharmacological inhibition of CIP2A with TD52 suppressed osteoclast differentiation and bone resorption both in vitro and in vivo, without causing major organ toxicity or affecting osteoblast function.

Conclusions

Our findings identify a novel CIP2A–OTUD4–HMGA1–c-Myc–PI3K/AKT regulatory axis that drives pathological osteoclastogenesis and bone loss. CIP2A represents a promising druggable target for

osteoporosis and related osteolytic diseases. As a potential first-in-class CIP2A inhibitor, TD52 merits further preclinical development for the treatment of postmenopausal osteoporosis.

Background

Osteoporosis is a chronic skeletal disorder in which bones gradually lose density and structural integrity, substantially raising the likelihood of fractures and related health complications. As global populations age, the condition has become a major public health challenge, affecting over 200 million individuals worldwide and imposing significant economic burdens [1, 2]. Normal bone health depends on a carefully regulated interplay between osteoblast-mediated bone formation and osteoclast-driven bone resorption [3]. Disruption of this balance, particularly through excessive osteoclast activity, is a key contributor to pathological bone loss.

Osteoclasts, derived from monocyte–macrophage precursors, are multinucleated cells whose differentiation is driven by macrophage colony-stimulating factor (M-CSF) and the receptor activator of nuclear factor-κB ligand (RANKL). Binding of RANKL to RANK recruits adaptor molecules such as TRAF6, activating downstream cascades including NF-κB, MAPK, and PI3K/AKT [4, 5]. These pathways collectively regulate transcription factors like NFATc1 and c-Fos, orchestrating osteoclast-specific gene expression and promoting bone resorption [6, 7]. Recent studies further reveal that osteoclast formation is governed not only at the transcriptional level but also through metabolic reprogramming and the integration of signaling networks, with the PI3K/AKT pathway serving as a critical hub that connects extracellular signals to cellular metabolism and survival [6, 8].

Although anti-resorptive therapies, such as bisphosphonates and denosumab, are widely used to treat osteoporosis, their long-term application is linked to serious adverse effects, such as atypical fractures and osteonecrosis of the jaw [9, 10]. These limitations underscore an unmet clinical need for novel therapeutic strategies that more precisely modulate osteoclast activity while ideally preserving or enhancing osteoblast function. Therapeutic strategies with such selectivity may offer superior outcomes for maintaining skeletal health.

CIP2A is an endogenous inhibitor of the tumor suppressor phosphatase PP2A and has been extensively characterized in cancer biology [11]. By inhibiting PP2A activity, CIP2A stabilizes phosphorylated substrates and amplifies oncogenic signaling pathways, including MYC and mTORC1 signaling [12]. CIP2A is frequently overexpressed in different cancers and is linked to unfavorable clinical outcomes [13, 14]. In addition, CIP2A has been implicated in diseases involving dysregulated phosphorylation signaling, including neurodegenerative disorders [15, 16]. However, its role in bone metabolism, particularly in osteoclast differentiation remains largely unexplored.

c-Myc serves as a key transcription factor that orchestrates cellular proliferation, differentiation, and metabolic reprogramming [17]. Emerging evidence demonstrates that c-Myc is essential for osteoclastogenesis, where it regulates mitochondrial oxidative phosphorylation and biosynthetic pathways required for osteoclast differentiation and function [18, 19]. Notably, c-Myc and the PI3K/AKT

signaling pathway form a reciprocal regulatory loop, in which c-Myc enhances PI3K/AKT signaling, whereas PI3K/AKT stabilizes c-Myc and promotes its transcriptional activity [20]. Despite these insights, the molecular events upstream of c-Myc that drive its expression in osteoclasts have yet to be clearly elucidated.

HMGA1 is a non-histone chromatin architectural protein that modulates gene transcription by altering chromatin conformation and facilitating transcriptional complex assembly [21]. HMGA1 plays critical roles in development, tumor progression, and metabolic regulation [22]. Recent studies suggest that HMGA1 also participates in skeletal biology, particularly in osteoblast differentiation [23]. However, its role in osteoclast differentiation and its potential involvement in regulating c-Myc transcription remain unclear.

Protein ubiquitination and deubiquitination constitute a dynamic regulatory system controlling protein stability and function. Deubiquitinating enzymes (DUBs) remove ubiquitin chains and thereby prevent proteasomal degradation of target proteins [24]. Increasing evidence indicates that ubiquitin-mediated regulation plays a critical role in bone remodeling [25]. OTUD4, a member of the OTU family, specifically cleaves K48-linked ubiquitin chains and regulates protein stability in immune and tumor-related processes [26, 27]. However, its function in osteoclast biology remains unknown.

Here, we define CIP2A as a previously unrecognized regulator governing osteoclast differentiation that mediates a deubiquitination-dependent signaling cascade. Mechanistically, CIP2A recruits OTUD4 to stabilize HMGA1 by preventing its ubiquitin-mediated degradation, thereby enhancing HMGA1-driven c-Myc transcription and establishing a positive feedback loop with PI3K/AKT signaling to amplify osteoclastogenesis and bone resorption.

To test this model, we employed in vitro osteoclast differentiation systems and an osteoporotic mouse model following ovariectomy (OVX) to systematically investigate the role of CIP2A in osteoclastogenesis and bone loss. Our study delineates a previously uncharacterized CIP2A-OTUD4-HMGA1-c-Myc-PI3K/AKT signaling axis, offering mechanistic insights into osteoclast regulation and identifying CIP2A as a potential therapeutic target for osteoporosis. Importantly, we also evaluate the therapeutic efficacy of TD52, a small-molecule CIP2A inhibitor, in preclinical models, providing a foundation for future translational development of CIP2A-targeted therapies for postmenopausal osteoporosis and related osteolytic diseases.

Materials and methods

Chemicals and reagents

All chemicals and reagents were of analytical purity. Small-molecule compounds, primary and secondary antibodies, assay kits, and other chemical reagents were purchased from commercial sources, with detailed product information (including names, suppliers, and catalog numbers) provided in

Supplementary Tables S1–S4. Protein extraction, Western blot, RT-qPCR, and ELISA related reagents were used per manufacturers' instructions.

Cell culture and osteoclast differentiation

Bone marrow macrophages (BMMs) were harvested from male C57BL/6 mice at 8 weeks of age [28] and maintained in α-MEM supplemented with 30 ng/mL M-CSF. To induce osteoclast formation, cells were plated at 2×10^4 per well in 96-well plates and exposed to 75 ng/mL RANKL along with M-CSF for 5–7 days, with the medium replaced each day. Differentiated osteoclasts were then identified by TRAP staining, and the number of multinucleated cells with at least three nuclei was recorded for analysis.

F-actin ring formation and bone resorption assay

To evaluate osteoclast function, differentiated BMMs were detached and reseeded onto Osteo Assay plates for 3 days. F-actin staining was performed by fixing, permeabilizing, and staining cells with rhodamine-phalloidin and DAPI. Images were acquired by fluorescence microscopy and quantified using ImageJ (version 1.53t, National Institutes of Health, USA). To assess bone resorption, cells were first eliminated with 5% sodium hypochlorite; then, the exposed resorption pits were visualized and measured.

Cell viability assay

BMMs were plated at 8×10^3 cells per well to assess cell viability using the CCK-8 assay. The cells were exposed to a range of TD52 concentrations (0–20 μM) and monitored on days 1, 3, and 5. At each time point, 10 μL of the CCK-8 reagent was introduced to the wells and incubated for 1 hour at 37°C. Absorbance at 450 nm was subsequently measured using a Bio-Tek microplate reader to assess cell proliferation.

Adenovirus infection

BMMs were infected with adenoviruses (MOI = 200) to modulate CIP2A expression, including Ad-CIP2A, Ad-shCIP2A, and respective controls. Following a 6-hour incubation in serum-free medium, the cells were subsequently maintained in complete medium for 48 hours. Gene modulation efficiency was verified by Real-time quantitative PCR (RT-qPCR) and Western blot.

OVX mouse model and in vivo treatment

All animal experiments received approval from the institutional ethics committee (TJH-202504009). Female C57BL/6 mice (12 weeks) were subjected to OVX or sham surgery. After 1 week, TD52 (10 mg/kg) was given orally 5 times/week for 8 weeks. For systemic gene regulation, AAV-shCIP2A or AAV-

CIP2A (150 μL, 1×10^{12} vg/mL) was administered via tail vein injection. For rescue experiments, AAV-c-Myc or the AKT agonist 740 Y-P was co-administered through the same route. At the endpoint, femurs, serum, and major organs (heart, liver, kidneys) were harvested for further analyses.

Micro-CT and histomorphometry

Femurs were fixed and analyzed by Micro-CT (Scanco Medical; 100 kV, 98 μA, 10 μm). The region of interest consisted of trabecular bone located 0.1 mm distal to the growth plate, covering a length equal to 5% of the femur. Quantitative assessment included bone volume fraction (BV/TV), trabecular number (Tb. N), trabecular thickness (Tb. Th), and trabecular separation (Tb. Sp). Decalcified sections (5 μm) were subjected to TRAP staining or immunofluorescence analysis.

RT-qPCR

TRIzol reagent was used for RNA extraction, followed by cDNA synthesis via reverse transcription. RT-qPCR analysis was carried out with SYBR Green chemistry using a protocol consisting of an initial step at 95°C for 5 min, then 40 repeated cycles of denaturation at 95°C for 10 s and extension at 60°C for 30 s. Relative mRNA levels were normalized to β-actin and calculated according to the 2^(-ΔΔCt) formula. Detailed primer information is available in Supplementary Table S5.

Western blot

Cell proteins were extracted with RIPA buffer, separated by SDS-PAGE, and electrotransferred onto PVDF membranes. After blocking, membranes were incubated with primary and secondary antibodies. Signals were detected using ECL and quantified relative to β-actin.

RNA-seq

BMMs were infected with Ad-shCIP2A or Ad-shCON and stimulated with RANKL for 3 days. RNA was extracted from three independent biological replicates and sequenced on an Illumina NovaSeq 6000 platform. Reads were mapped to the mouse genome (GRCm38), and differentially expressed genes were identified using edgeR (FDR ≤ 0.05, $|\log_2 FC| > 1$), followed by Gene Set Enrichment Analysis (GSEA) and Kyoto Encyclopedia of Genes and Genomes (KEGG) analyses.

Immunofluorescence

Cells underwent fixation, permeabilization, and blocking prior to antibody staining. Primary antibodies were applied followed by fluorescently labeled secondary antibodies. Nuclear staining was achieved with DAPI. Images were obtained using a fluorescence microscope and quantified with ImageJ.

Co-IP

Cell lysates were prepared in IP buffer, and 500 μg of protein was incubated with 2 μg anti-CIP2A or control IgG at 4°C overnight. Immune complexes were captured using Protein A/G magnetic beads for 4 h. After extensive washing, proteins were eluted by boiling in loading buffer and subjected to Western blot analysis for HMGA1 and OTUD4.

IP-MS

To identify the CIP2A interactome, cell lysates (1–2 mg) were immunoprecipitated with anti-CIP2A or control IgG. The bead-bound proteins were digested on-bead and analyzed by LC-MS/MS, and label-free quantification was used to identify specifically enriched proteins.

ChIP-seq

BMMs induced with RANKL for 3 days were crosslinked using 1% formaldehyde for 10 min, quenched with glycine, and lysed. Chromatin was sheared to 200–500 bp by sonication and immunoprecipitated with anti-HMGA1 or control IgG. Libraries were prepared from three independent biological replicates and sequenced on an Illumina NovaSeq 6000 platform. Reads were aligned to the mouse genome (GRCm38), peaks called with MACS2 (FDR < 0.05), and motif analysis performed using HOMER.

ChIP-qPCR

ChIP DNA was analysed by qPCR with primers specific for the HMGA1 binding region of the c-Myc gene identified by ChIP-seq. Data were normalised to input chromatin and expressed as fold enrichment relative to the IgG control, thereby confirming specific HMGA1 occupancy at the c-Myc locus.

Dual-luciferase reporter assay

BMMs were co-transfected with pGL3-c-Myc-WT or -MUT, HMGA1 overexpression or empty control plasmid, and pRL-TK with Lipofectamine 3000. Following 24–48 hours, cells were lysed, and Firefly and Renilla luciferase activities were sequentially measured with a dual-luciferase assay system. Results were expressed as the Firefly/Renilla ratio.

CHX chase assay

To assess HMGA1 protein stability, BMMs with CIP2A knockdown were treated with 50 μg/mL CHX to inhibit new protein synthesis. Cells were collected at 0, 2, 4, 6, and 8 hours after CHX addition. HMGA1 levels were quantified by Western blot, and band intensities were normalized to β-actin. The degradation rate was determined by plotting the remaining HMGA1 protein over time.

Ubiquitination assay

Cells received a 6-hour pretreatment with the proteasome inhibitor MG132 (10 μM) to block degradation. HMGA1 was then immunoprecipitated and immunoblotted with anti-ubiquitin to assess its ubiquitination levels.

Osteoblastogenesis assay

MC3T3-E1 cells (subclone 14) were seeded in 24-well plates at 5×10^4 cells per well and cultured in osteogenic medium containing 100 nM dexamethasone, 50 μg/mL ascorbic acid, and 5 mM β-glycerophosphate. Cells were infected with Ad-CIP2A/Ad-shCIP2A or treated with TD52 (0–10 μM). ALP activity was evaluated on day 7, and mineral deposition was assessed by Alizarin Red S (ARS) staining on day 21. Images were captured under light microscopy.

Enzyme-linked immunosorbent assay (ELISA)

Blood samples were collected via the retro-orbital sinus, and serum was obtained by centrifugation (2000 rpm, 30 min, 4°C). Levels of PINP and CTX-1 were determined using ELISA kits following the manufacturers' instructions.

Statistics

Experiments were repeated independently at least three times. Data are shown as mean ± SD. Statistical analyses were performed using GraphPad Prism 9.5. Comparisons between two groups were conducted using an unpaired two-tailed Student's t-test, while multiple groups were analyzed by one-way ANOVA with Tukey's post hoc test. Statistical significance was defined as p value < 0.05 (*p < 0.05, **p < 0.01).

Results

CIP2A is upregulated during osteoclast differentiation

To explore the potential involvement of CIP2A in osteoclastogenesis, we first examined single-cell transcriptomic datasets from the TISCH database [29]. CIP2A exhibited a differentiation stage–dependent expression pattern within the myeloid lineage, with low expression in monocytes/macrophages and markedly higher expression in terminally differentiated neutrophils (Fig. 1A–C). Given that osteoclasts originate from the monocyte/macrophage lineage, this pattern suggested a potential upregulation of CIP2A during differentiation. Consistently, RNA-seq analysis revealed that RANKL stimulation significantly induced CIP2A transcription in BMMs (Fig. 1D). Analysis of the BioGPS database (1449699_s_at) further confirmed elevated CIP2A expression in osteoclasts (Fig. 1E).

We next validated these findings experimentally. Both RT-qPCR and western blot demonstrated a time-dependent increase in the mRNA and protein expression of CIP2A throughout osteoclast differentiation (days 0–5) (Fig. 1F–H). Immunofluorescence analysis further confirmed progressive accumulation of CIP2A signal as differentiation proceeded (Fig. 1I). Together, these data consistently demonstrate that CIP2A is dynamically upregulated during osteoclastogenesis, implicating a potential functional role in this process.

CIP2A promotes osteoclast differentiation and bone resorption in vitro

To determine the functional role of CIP2A, we established both loss- and gain-of-function models using adenoviral systems. Efficient knockdown of CIP2A was validated using RT-qPCR and western blot (Fig. 2A, B). TRAP staining showed a marked decrease in osteoclast count upon CIP2A silencing (Fig. 2C). Moreover, F-actin staining showed impaired actin ring formation (Fig. 2D), accompanied by a significant decrease in bone resorption activity (Fig. 2E). Consistently, expression of osteoclast functional markers CTSK and MMP9 was notably reduced (Fig. 2F, G).

Conversely, CIP2A overexpression robustly enhanced osteoclast formation (Fig. 2J), promoted actin ring formation (Fig. 2K), and increased resorptive capacity (Fig. 2L), accompanied by elevated expression of CTSK and MMP9 (Fig. 2M, N). Collectively, these findings indicate that CIP2A functions as a positive modulator of osteoclast differentiation and function in vitro.

CIP2A regulates OVX-induced bone loss in vivo

To investigate the in vivo relevance of CIP2A, we employed an OVX-induced osteoporosis model. Adeno-associated virus (AAV) vectors encoding shCip2a or Cip2a cDNA were administered via tail vein injection to achieve systemic gene silencing or overexpression, respectively (Fig. 3A).

Immunofluorescence staining confirmed that AAV-shCIP2A effectively reduced, while AAV-CIP2A increased, the proportion of $CTSK^+$ $CIP2A^+$ cells, confirming effective knockdown and overexpression of CIP2A in osteoclasts (Fig. 3B, C). AAV-shCIP2A significantly mitigated OVX-induced trabecular bone loss, as shown by Micro-CT reconstruction (Fig. 3D). Quantitative analysis revealed higher BV/TV, Tb. N, and Tb. Th, along with lower Tb. Sp (Fig. 3E). Histological analysis of TRAP-stained femoral sections further confirmed a reduction in osteoclast number and surface following CIP2A knockdown (Fig. 3F, G).

Conversely, AAV-mediated CIP2A overexpression exacerbated bone loss (Fig. 3H), accompanied by decreased BV/TV, Tb. N, Tb. Th, and increased Tb. Sp (Fig. 3I), as well as elevated osteoclast parameters (Fig. 3J, K). These findings demonstrate that CIP2A promotes bone resorption in vivo and contributes to osteoporotic bone loss.

Pharmacological inhibition of CIP2A by TD52 suppresses osteoclastogenesis and bone loss

To assess the translational potential of targeting CIP2A, we examined TD52, a small-molecule inhibitor of CIP2A. In BMM cultures, TD52 did not influence cell viability across the tested concentrations (Fig. 4A). TRAP staining showed that TD52 suppressed osteoclast formation in a concentration-dependent manner (Fig. 4B, C). F-actin ring assembly and bone resorption activity were similarly inhibited by TD52 treatment (Fig. 4D–G).

We then administered TD52 to OVX mice (Fig. 4H). Micro-CT analysis indicated that TD52 administration in OVX mice significantly ameliorated trabecular bone structure (Fig. 4J), as confirmed by increased BV/TV, Tb. Th, and Tb. N along with decreased Tb. Sp (Fig. 4K). TRAP staining confirmed a marked reduction in osteoclast numbers on trabecular surfaces following TD52 treatment (Fig. 4L, M). Notably,

histopathological evaluation of key organs (heart, liver, kidney) revealed no discernible pathological changes, indicating favorable in vivo tolerability (Fig. 4I). These findings identify pharmacological CIP2A inhibition as an effective strategy to restrain osteoclast activity and mitigate bone loss.

CIP2A stabilizes HMGA1 by recruiting the deubiquitinase OTUD4

To elucidate the molecular mechanism through which CIP2A drives osteoclast differentiation, we carried out IP-MS to identify CIP2A-interacting proteins. Among the top candidates were HMGA1 and the deubiquitinase OTUD4 (Fig. 5A). Co-IP assays confirmed that CIP2A associates with both OTUD4 and HMGA1 (Fig. 5B). Immunofluorescence co-localization analysis revealed cytoplasmic colocalization of CIP2A and OTUD4, whereas HMGA1 was primarily nuclear (Fig. 5C), suggesting that HMGA1 stability may be regulated prior to nuclear translocation.

Notably, CIP2A overexpression enhanced the interaction between OTUD4 and HMGA1 (Fig. 5D, E), indicating a scaffolding role for CIP2A. Given OTUD4's known deubiquitinating activity, we examined HMGA1 ubiquitination and turnover. CIP2A knockdown markedly increased HMGA1 polyubiquitination (Fig. 5F) and accelerated HMGA1 degradation in CHX chase assays (Fig. 5G, H). CIP2A modulation had no impact on Hmga1 mRNA levels (Fig. 5I), confirming regulation at the post-translational level. Concordantly, CIP2A overexpression elevated HMGA1 protein abundance (Fig. 5J, K). Functionally, HMGA1 silencing attenuated the pro-osteoclastogenic effect of CIP2A overexpression (Fig. 5L–O), establishing HMGA1 as a critical downstream effector of CIP2A. Collectively, these results demonstrate that CIP2A serves as a molecular bridge that recruits OTUD4 to remove ubiquitin chains from HMGA1, thereby stabilizing HMGA1 and driving osteoclast differentiation.

The CIP2A–HMGA1 axis activates c-Myc transcription

To define the transcriptional consequences of CIP2A–HMGA1 signaling, we integrated RNA-seq data from CIP2A-depleted BMMs with HMGA1 ChIP-seq profiles. RNA-seq revealed that c-Myc was among the genes significantly downregulated upon CIP2A knockdown (Fig. 6A, B). ChIP-seq analysis showed broad HMGA1 binding across the genome, with enrichment at intergenic and intronic regions, suggesting regulation via distal regulatory elements (Fig. 6C, D). Intersection of ChIP-seq and RNA-seq data revealed 63 putative HMGA1 target genes, with c-Myc ranking prominently among them (Fig. 6E, F).

Visualization of ChIP-seq signal tracks confirmed robust HMGA1 binding peaks within the c-Myc locus (Fig. 6G), and motif analysis revealed enrichment of HMGA1 consensus sequences in c-Myc-associated regulatory regions (Fig. 6H). ChIP-qPCR confirmed that CIP2A overexpression significantly enhanced HMGA1 occupancy at the c-Myc regulatory region, and agarose gel electrophoresis of ChIP-qPCR products confirmed amplicon specificity (Fig. 6I, J). Luciferase reporter assays demonstrated that HMGA1 overexpression activated a c-Myc promoter/5'UTR-driven reporter, an effect that was attenuated by mutation of the putative HMGA1 binding site (Fig. 6K). Consistently, CIP2A overexpression increased

c-Myc mRNA and protein levels, which was partially reversed following HMGA1 knockdown (Fig. 6L–N). These findings indicate that CIP2A facilitates c-Myc transcription through HMGA1 stabilization.

A c-Myc–PI3K/AKT positive feedback loop amplifies CIP2A-mediated osteoclastogenesis

Pathway enrichment analysis of DEGs following CIP2A knockdown highlighted significant enrichment of the PI3K/AKT signaling pathway (Fig. 7A–C). Consistent with this, CIP2A knockdown attenuated RANKL-induced AKT phosphorylation, whereas c-Myc overexpression restored it (Fig. 7D, E).

Functionally, c-Myc overexpression partially rescued the osteoclast formation defect caused by CIP2A knockdown, an effect abolished by the PI3K inhibitor LY294002 (Fig. 7F, G). Similar trends were observed for osteoclast marker expression (Fig. 7H, I). Conversely, the c-Myc inhibitor 10058-F4 suppressed CIP2A overexpression-driven osteoclast differentiation, an effect partially reversed by the AKT activator 740 Y-P (Fig. 7J-M).

Western blot analysis further revealed that 740 Y-P upregulated, whereas LY294002 downregulated, c-Myc protein levels (Fig. 7N, O). These data unveil a positive feedback loop wherein c-Myc activates the PI3K/AKT pathway, and PI3K/AKT signaling in turn reinforces c-Myc expression, thereby amplifying osteoclastogenesis downstream of CIP2A.

Targeting the CIP2A–HMGA1–c-Myc axis mitigates bone loss via PI3K/AKT signaling in vivo

Finally, in vivo rescue experiments were performed to confirm the functional hierarchy of the CIP2A-HMGA1-c-Myc signaling axis in bone metabolism. Micro-CT analysis showed that the protective effect of CIP2A knockdown on OVX-induced trabecular bone loss was partially reversed by either overexpression of c-Myc or administration of the AKT activator 740 Y-P (Fig. 8A, B). Histomorphometric analysis confirmed that the reduction in osteoclast numbers achieved by CIP2A silencing was largely negated by c-Myc overexpression or AKT activation (Fig. 8C, D). These findings establish that the CIP2A–HMGA1–c-Myc axis drives osteoclast-mediated bone resorption through PI3K/AKT signaling.

CIP2A modulation and TD52 treatment do not affect osteogenic differentiation

To evaluate the effects of CIP2A modulation and TD52 on osteoblast differentiation, MC3T3-E1 cells were treated with Ad-CIP2A, Ad-shCIP2A, or TD52 (0–10 μM). ALP and ARS staining showed no differences in enzymatic activity or mineralization (Supplementary Fig. S1A–D, L–M). Similarly, qPCR and Western blot analyses indicated unchanged expression of osteoblast markers RUNX2 and ALP (Supplementary Fig. S1E–G). In vivo, OCN immunohistochemistry revealed comparable osteoblast densities among AAV-CIP2A, AAV-shCIP2A, and control mice (Supplementary Fig. S1H–I), and serum

P1NP levels were unaltered (Supplementary Fig. S1J). These findings suggest that CIP2A modulation and TD52 primarily exert their bone-protective effects through osteoclast inhibition.

Discussion

The present study establishes CIP2A as a pivotal upstream modulator of osteoclast differentiation and bone resorption via the OTUD4–HMGA1–c-Myc–PI3K/AKT axis (Fig. 9), highlighting its translational potential as a therapeutic target for osteoporosis. Multi-omics analyses and functional validation demonstrate that CIP2A positively regulates osteoclast formation, revealing an unexpected link between tumor-associated signaling and skeletal homeostasis that can be pharmacologically exploited. Importantly, systemic AAV-mediated CIP2A modulation and TD52 treatment did not affect osteoblast differentiation, as shown by ALP/ARS staining, RUNX2 and ALP expression, OCN immunohistochemistry, and serum P1NP levels. These findings suggest that CIP2A inhibition exerts bone-protective effects primarily through osteoclast suppression rather than direct actions on osteoblasts, a desirable feature for an anti-resorptive agent with fewer side effects. Mechanistically, CIP2A stabilizes HMGA1 via OTUD4 recruitment, enabling nuclear translocation and activation of c-Myc, which forms a positive feedback loop with PI3K/AKT to drive osteoclastogenesis. Targeting this circuit using the small-molecule inhibitor TD52 effectively inhibits osteoclast activity without impairing osteoblast function, providing a viable therapeutic strategy for postmenopausal osteoporosis and other osteolytic diseases. Moreover, the cross-disciplinary implication of CIP2A, previously characterized in cancer biology [30, 31], highlights its potential as a shared regulatory node bridging tumor progression and bone destruction, which may have implications for cancer-induced bone loss.

A key mechanistic insight from this work lies in the coupling between cytoplasmic protein quality control and HMGA1-mediated nuclear transcription. From a translational standpoint, this mechanism offers a distinct intervention point – stabilizing or destabilizing HMGA1 via its deubiquitination – that could be targeted by future small molecules. Although HMGA1 is traditionally regarded as a nuclear architectural transcription factor [32], our data support a two-stage regulatory model in which its functional competence is primed in the cytoplasm. Specifically, CIP2A functions as a molecular scaffold that recruits the deubiquitinase OTUD4, thereby suppressing HMGA1 ubiquitination and proteasomal degradation. OTUD4, recently implicated in immune signaling and tumor microenvironment regulation [26, 27], has not been previously linked to bone homeostasis; our study thus expands its functional repertoire into the skeletal system. This is in line with the broader role of ubiquitination in protein stability and disease regulation [25, 33]. Such cytoplasmic stabilization ensures efficient nuclear translocation of HMGA1, establishing a spatially coordinated regulatory mechanism reminiscent of other transcription factors controlled by post-translational modifications prior to nuclear entry, such as p53 and β-catenin [34, 35].

Once stabilized and translocated into the nucleus, HMGA1 exerts its function as an architectural transcription factor. At the chromatin level, our findings further refine the understanding of HMGA1-mediated transcriptional regulation by emphasizing its role in long-range gene control. ChIP-seq data

revealed preferential binding of HMGA1 to distal regulatory regions rather than canonical promoters, consistent with its function as an architectural transcription factor orchestrating chromatin topology [21, 36]. This observation aligns with recent advances in enhancer biology, where distal regulatory elements and three-dimensional chromatin interactions play central roles in gene activation [37]. In this context, HMGA1 likely facilitates enhancer–promoter looping to activate c-Myc transcription, thereby linking chromatin organization to osteoclastogenic gene expression programs. Beyond osteoclast biology, this study highlights a generalizable paradigm in which cytoplasmic protein stabilization governs nuclear transcriptional competence, bridging post-translational regulation with chromatin architecture – a concept that may inform future therapeutic strategies targeting transcriptional dependencies in bone diseases .

Given that HMGA1 primarily functions as a chromatin architectural regulator rather than a direct transcriptional activator, identifying its critical downstream effector is essential. In this context, c-Myc emerged as the central mediator. The identification of c-Myc was supported by a multi-layered selection strategy integrating transcriptomic changes, chromatin occupancy, and functional relevance. c-Myc has been extensively implicated in metabolic reprogramming and proliferative control [38], and its role in osteoclast differentiation has been increasingly appreciated [19]. In our study, c-Myc fulfilled key criteria, including transcriptional responsiveness to CIP2A modulation, direct regulation by HMGA1, and central positioning within the signaling network. This reinforces the concept that osteoclastogenesis requires metabolic reprogramming, and positions c-Myc as a critical integrator of upstream signaling and downstream functional output – a nexus with potential therapeutic relevance .

Importantly, we demonstrate that c-Myc forms a positive feedback loop with the PI3K/AKT signaling pathway, a key axis in osteoclast biology [39]. c-Myc enhances PI3K/AKT activation, while activated AKT in turn stabilizes and upregulates c-Myc, creating a self-reinforcing circuit. Such feedback loops are known to amplify signaling strength and confer robustness to biological processes, particularly in terminal differentiation systems [40]. In the context of osteoporosis, this loop may contribute to sustained osteoclast activation under pathological stimuli, thereby exacerbating bone loss. These results imply that interfering with this feedback circuit may provide a more effective therapeutic benefit than blocking individual components alone.

From a translational perspective, the CIP2A inhibitor TD52 exhibits promising inhibitory effects on osteoclastogenesis and bone resorption both in vitro and in vivo without overt toxicity, making it a lead candidate for further preclinical development. Compared with current anti-resorptive therapies such as bisphosphonates or denosumab, targeting CIP2A offers an upstream intervention strategy that may prevent compensatory activation of downstream pathways. TD52 is known to inhibit CIP2A-PP2A interaction [30]; whether it disrupts CIP2A-OTUD4-HMGA1 complex formation warrants further study. However, several challenges remain before clinical application. The specificity of TD52 toward CIP2A requires further validation, particularly given the widespread involvement of CIP2A in multiple physiological and pathological processes. Additionally, pharmacokinetic properties, long-term safety, and potential off-target effects need to be systematically evaluated in future translational studies.

Despite the merits of this study, certain limitations must be recognized. First, the precise structural basis of the CIP2A–OTUD4–HMGA1 interaction remains unclear and warrants further investigation using structural and biophysical approaches. Second, our in vivo conclusions rely heavily on systemic AAV-mediated gene manipulation via tail vein injection and the OVX model; therefore, future studies should incorporate genetic knockout models as well as diverse osteoporosis models, such as glucocorticoid-induced, inflammation-induced, and aging-related bone loss, to enhance the robustness and generalizability of our findings. Third, this study focuses mainly on osteoclasts, and future work should explore the role of CIP2A in the broader bone microenvironment, including osteoblast–osteoclast crosstalk. Finally, potential crosstalk between the CIP2A axis and other signaling cascades, including Wnt/β-catenin or mTOR, remains to be elucidated. Addressing these questions will be crucial for translating our mechanistic insights into novel therapeutic strategies for osteoporosis and related osteolytic diseases.

In summary, we define a previously unrecognized CIP2A-centered regulatory axis that integrates cytoplasmic protein stabilization, chromatin architecture, and signaling feedback to control osteoclast differentiation. This work not only advances the mechanistic understanding of bone resorption but also establishes CIP2A as a potential therapeutic candidate for osteoporosis, with TD52 as a promising lead compound for further translational development.

Abbreviations

AAV: adeno-associated virus

α-MEM: alpha modified minimal essential medium

BMMs: bone marrow-derived macrophages;

BV/TV: bone volume per tissue

CCK-8: cell counting kit-8

CHX: cycloheximide

ChIP: Chromatin Immunoprecipitation

CIP2A: cancerous inhibitor of protein phosphatase 2A

Co-IP: co-immunoprecipitation

CTSK: cathepsin K

GSEA: Gene Set Enrichment Analysis

HMGA1: high mobility group A1

IP-MS: Immunoprecipitation-Mass Spectrometry

KEGG: Kyoto Encyclopedia of Genes and Genomes

M-CSF: macrophage colony-stimulating factor

MMP-9: matrix metalloproteinase 9

NF-κB: nuclear factor kappa B

N.Oc/B. Pm: osteoclasts per bone perimeter

O. Oc. N/BS: osteoclast number per bone surface

OTUD4: OTU deubiquitinase 4

OVX: ovariectomy

P1NP: Procollagen type I N-terminal propeptide

PI3K/AKT: phosphatidylinositol 3-kinase/protein kinase B

RANKL: receptor activator of nuclear factor κB ligand

RNA-seq: RNA sequencing

RT-qPCR: real-time quantitative PCR

TRAP: Tartrate-resistant acid phosphatase

Tb. N: trabecular bone numbers

Tb. Th: trabecular bone thickness

Tb. Sp: trabecular.

Declarations

Ethics Statement

All animal experiments received approval from Tongji Hospital Ethics Committee of Huazhong University of Science and Technology (TJH-202504009) and were performed in compliance with ARRIVE guidelines.

Consent for publication

Not applicable.

Data Availability Statement

The raw data used or analysed in the study are available from the corresponding author on reasonable request.

Competing interest

The authors declare no competing interests.

Funding Statement

This work was supported by the National Natural Science Foundation of China (Grant no. 82572839, 82502923) and Hubei Province Natural Science Foundation (Grant no. 2024AFB608).

Author contributions

M.Z., J.L., and X.S. conceptualized the study; M.Z., Y.D., Y.Z., S.W., and J.L. developed methodology; M.Z., J.H., J.L., S.W., and Y.M. performed investigation; M.Z., J.H., and J.L. curated data; M.Z. wrote the original draft; J.L., Y.M., J.L., F.L., and X.S. reviewed and edited the manuscript; F.L., J.H., and X.S. supervised and acquired funding; H.K., Y.D. and F.L. provided resources. All data in-house, no paper mill used. All authors agree to be accountable.

Acknowledgements

We extend our gratitude to all members of the Orthopedic Research Institute at Tongji Hospital for their technical support and constructive discussions.

References

1. Compston JE, McClung MR, Leslie WD. Osteoporos Lancet. 2019;393(10169):364–76.
2. Feng X, McDonald JM. Disorders of bone remodeling. Annu Rev Pathol. 2011;6:121–45.
3. Dong Q, Fu H, Li W, Ji X, Yin Y, Zhang Y, et al. Nuclear farnesoid X receptor protects against bone loss by driving osteoblast differentiation through stabilizing RUNX2. Bone Res. 2025;13(1):20.
4. Wang M, Yuan C, Zhang Y, Peng M, Liu Y, Liu R et al. Moonlighting cytosolic function of ACAD9: suppression of TRAF6-mediated osteoclastogenesis and protection against osteoporosis. Cell Death Dis. 2026;17(1).
5. Bai C, Zhang M, Liu L, Tao L, Xu C, Chai H, et al. Galphai1/3 Is a Novel Regulatory Target for RANKL Signal Transduction and Osteoporosis. Adv Sci (Weinh). 2026;13(20):e10836.
6. de Molon RS, Vernal R, Oliveira GE, Steffens JP, Ervolino E, Theodoro LH, et al. Inflammatory bone loss and signaling pathways in periodontitis: mechanistic insights and emerging therapeutic strategies. Bone Res. 2026;14(1):1.

7. Yokota K, Sato K, Miyazaki T, Aizaki Y, Tanaka S, Sekikawa M, et al. Characterization and Function of Tumor Necrosis Factor and Interleukin-6-Induced Osteoclasts in Rheumatoid Arthritis. Arthritis Rheumatol. 2021;73(7):1145–54.
8. Tang R, Liu G, Wang C, Chao M, Ma G, Wei P, et al. Transcriptomics Guided Engineering of Exosome-Encapsulated Bifunctional Nanosheets Targeting the Immune-PI3K/Akt Axis for Osteoporosis Therapy. Adv Sci (Weinh). 2025;12(47):e11327.
9. Reid IR, Horne AM, Mihov B, Bava U, Stewart A, Gamble GD. Duration of fracture prevention after zoledronate treatment in women with osteopenia: observational follow-up of a 6-year randomised controlled trial to 10 years. Lancet Diabetes Endocrinol. 2024;12(4):247–56.
10. Reid IR, Billington EO. Drug therapy for osteoporosis in older adults. Lancet. 2022;399(10329):1080–92.
11. Neale DA, Morris JC, Verrills NM, Ammit AJ. Understanding the regulatory landscape of protein phosphatase 2A (PP2A): Pharmacological modulators and potential therapeutics. Pharmacol Ther. 2025;269:108834.
12. Routila E, Mahran R, Salminen S, Irjala H, Haapio E, Kyto E, et al. Identification of stemness-related glycosylation changes in head and neck squamous cell carcinoma. BMC Cancer. 2024;24(1):443.
13. Jeong IH, Yun JK, Jin JO, Lee GD, Lee PC. Ring Finger Protein 1, a Novel Ubiquitin E3 Ligase Targeting Cancerous Inhibitor of Protein Phosphatase 2A to Suppress Smoking-Induced Lung Tumorigenesis. MedComm (2020). 2025;6(12):e70522.
14. Laine A, Nagelli SG, Farrington C, Butt U, Cvrljevic AN, Vainonen JP, et al. CIP2A Interacts with TopBP1 and Drives Basal-Like Breast Cancer Tumorigenesis. Cancer Res. 2021;81(16):4319–31.
15. Khan MM, Ullah U, Khan MH, Kong L, Moulder R, Valikangas T, et al. CIP2A Constrains Th17 Differentiation by Modulating STAT3 Signaling. iScience. 2020;23(3):100947.
16. Liu N, He QM, Chen JW, Li YQ, Xu YF, Ren XY, et al. Overexpression of CIP2A is an independent prognostic indicator in nasopharyngeal carcinoma and its depletion suppresses cell proliferation and tumor growth. Mol Cancer. 2014;13:111.
17. Xia P, Zhang H, Lu H, Xu K, Jiang X, Jiang Y, et al. METTL5 stabilizes c-Myc by facilitating USP5 translation to reprogram glucose metabolism and promote hepatocellular carcinoma progression. Cancer Commun (Lond). 2023;43(3):338–64.
18. La T, Chen S, Guo T, Zhao XH, Teng L, Li D, et al. Visualization of endogenous p27 and Ki67 reveals the importance of a c-Myc-driven metabolic switch in promoting survival of quiescent cancer cells. Theranostics. 2021;11(19):9605–22.
19. Chen H, Li S, Yin H, Hua Z, Shao Y, Wei J, et al. MYC-mediated miR-320a affects receptor activator of nuclear factor kappaB ligand (RANKL)-induced osteoclast formation by regulating phosphatase and tensin homolog (PTEN). Bioengineered. 2021;12(2):12677–87.
20. Tao X, Li Y, Fan S, Wu L, Xin J, Su Y, et al. Downregulation of Linc00173 increases BCL2 mRNA stability via the miR-1275/PROCA1/ZFP36L2 axis and induces acquired cisplatin resistance of lung adenocarcinoma. J Exp Clin Cancer Res. 2023;42(1):12.

21. Olan I, Ando-Kuri M, Parry AJ, Handa T, Schoenfelder S, Fraser P et al. HMGA1 orchestrates chromatin compartmentalization and sequesters genes into 3D networks coordinating senescence heterogeneity. Nat Commun. 2024;15(1).
22. Chia L, Wang B, Kim JH, Luo LZ, Shuai S, Herrera I et al. HMGA1 induces FGF19 to drive pancreatic carcinogenesis and stroma formation. J Clin Invest. 2023;133(6).
23. Wu Z, Zhu J, Wen Y, Lei P, Xie J, Shi H, et al. Hmga1-overexpressing lentivirus protects against osteoporosis by activating the Wnt/beta-catenin pathway in the osteogenic differentiation of BMSCs. FASEB J. 2023;37(9):e22987.
24. Lange SM, Armstrong LA, Kulathu Y, Deubiquitinases. From mechanisms to their inhibition by small molecules. Mol Cell. 2022;82(1):15–29.
25. Fan X, Zhang R, Xu G, Fan P, Luo W, Cai C et al. Role of ubiquitination in the occurrence and development of osteoporosis (Review). Int J Mol Med. 2024;54(2).
26. Zhao Y, Mudge MC, Soll JM, Rodrigues RB, Byrum AK, Schwarzkopf EA, et al. OTUD4 Is a Phospho-Activated K63 Deubiquitinase that Regulates MyD88-Dependent Signaling. Mol Cell. 2018;69(3):505–e165.
27. Liang B, Hu A, Lu H, Zhou H, Chen Q, Jia C et al. OTUD4-ZMYND8-DDX3X Axis Drives Immunosuppressive Microenvironment in Spinal Metastases of Triple-Negative Breast Cancer. Neoplasia. 2026;71.
28. Zhu M, Guo Q, Kang H, Peng R, Dong Y, Zhang Y, et al. Inhibition of FAAH suppresses RANKL-induced osteoclastogenesis and attenuates ovariectomy-induced bone loss partially through repressing the IL17 pathway. FASEB Journal: Official Publication Federation Am Soc Experimental Biology. 2023;37(1):e22690.
29. Han Y, Wang Y, Dong X, Sun D, Liu Z, Yue J, et al. TISCH2: expanded datasets and new tools for single-cell transcriptome analyses of the tumor microenvironment. Nucleic Acids Res. 2023;51(D1):D1425–31.
30. Yu HC, Hung MH, Chen YL, Chu PY, Wang CY, Chao TT, et al. Erlotinib derivative inhibits hepatocellular carcinoma by targeting CIP2A to reactivate protein phosphatase 2A. Cell Death Dis. 2014;5(7):e1359.
31. Tinsley SL, Shelley RA, Mall GK, Chianis ERD, Dhiman A, Baral G et al. KRAS-mediated upregulation of CIP2A promotes suppression of PP2A-B56alpha to initiate pancreatic cancer development. bioRxiv. 2024.
32. Wang L, Zhang J, Xia M, Liu C, Zu X, Zhong J. High Mobility Group A1 (HMGA1): Structure, Biological Function, and Therapeutic Potential. Int J Biol Sci. 2022;18(11):4414–31.
33. Liao Y, Zhang W, Liu Y, Zhu C, Zou Z. The role of ubiquitination in health and disease. MedComm (2020). 2024;5(10):e736.
34. Liao Y, Liang J, Wang Y, Li A, Liu W, Zhong B, et al. Target deubiquitinase OTUB1 as a therapeatic strategy for BLCA via beta-catenin/necroptosis signal pathway. Int J Biol Sci. 2024;20(10):3784–801.

35. Su Y, Luo Y, Zhang P, Lin H, Pu W, Zhang H, et al. Glucose-induced CRL4(COP1)-p53 axis amplifies glycometabolism to drive tumorigenesis. Mol Cell. 2023;83(13):2316–e317.
36. Dudka D, Dawicki-McKenna JM, Sun X, Beeravolu K, Akera T, Lampson MA, et al. Satellite DNA shapes dictate pericentromere packaging in female meiosis. Nature. 2025;638(8051):814–22.
37. Kawasaki K, Fukaya T. Regulatory landscape of enhancer-mediated transcriptional activation. Trends Cell Biol. 2024;34(10):826–37.
38. Yegambaram M, Sun X, Lu Q, Flores AG, Zemskova M, Soto J, et al. c-Myc promotes metabolic reprogramming in pulmonary hypertension via the stimulation of glutaminolysis and the reductive tricarboxylic acid cycle. Redox Biol. 2025;85:103765.
39. Su X, Wang Q, Wang J, Zhu P, Guo W, Yang J, et al. Mesothelin as a biomarker and potential therapeutic target in rheumatoid arthritis bone destruction. Cell Rep Med. 2025;6(11):102430.
40. Stegen S, Moermans K, Stockmans I, Thienpont B, Carmeliet G. The serine synthesis pathway drives osteoclast differentiation through epigenetic regulation of NFATc1 expression. Nat Metab. 2024;6(1):141–52.

Figures

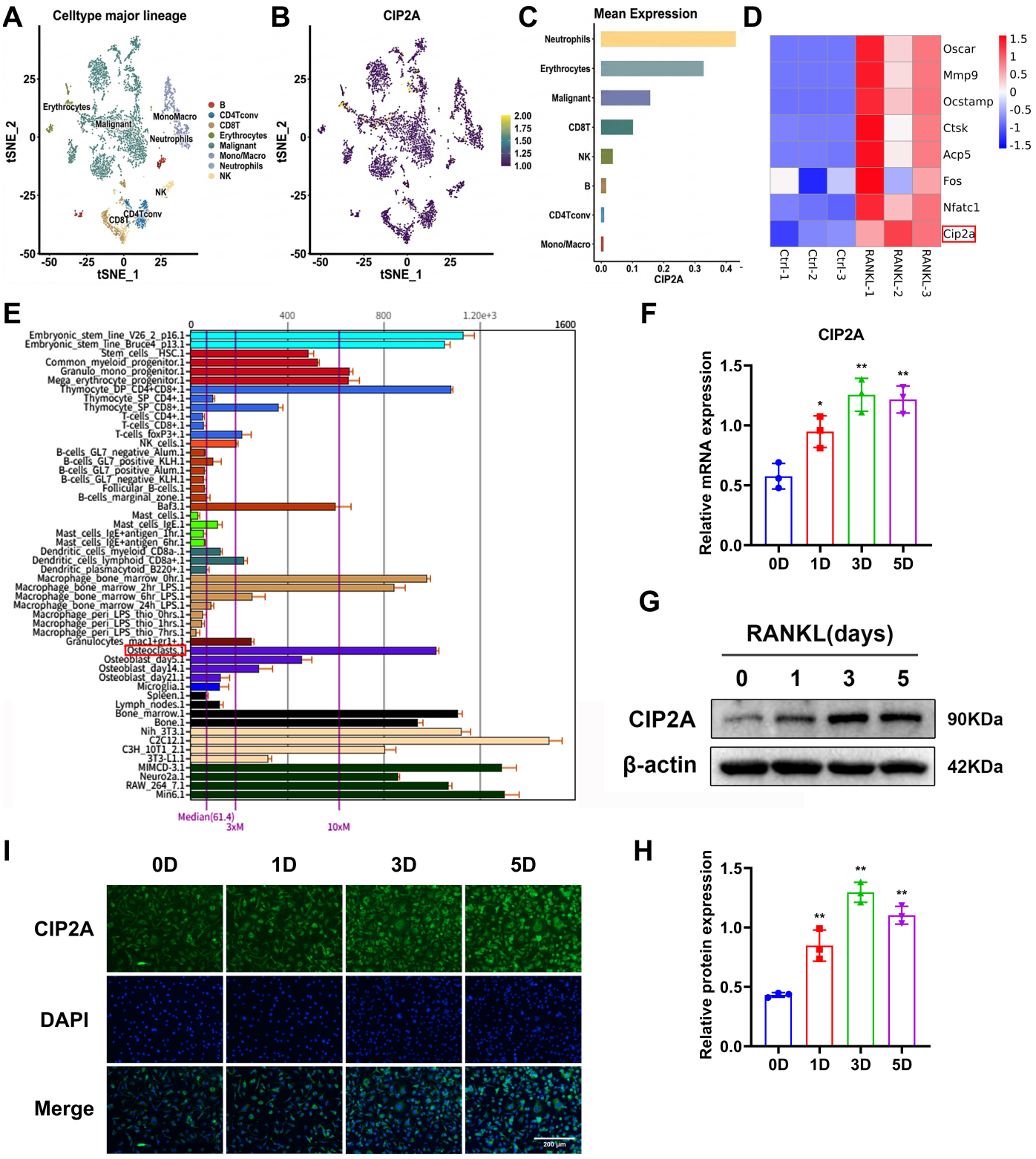


Figure 1

CIP2A expression during osteoclast differentiation. (A–C) Single-cell transcriptomic analysis from TISCH showing CIP2A expression across myeloid differentiation stages, with higher levels in terminally differentiated neutrophils compared to immature monocytes/macrophages. (D) RNA-seq heatmap showing elevated Cip2a transcript levels in RANKL-stimulated BMMs. (E) BioGPS analysis indicating high CIP2A expression in osteoclasts. (F–I) RT-qPCR, Western blot, and immunofluorescence showing

time-dependent increases in Cip2a mRNA and CIP2A protein during a 5-day osteoclast differentiation. Data are presented as mean ± SD. N = 3 independent experiments. Scale bar: 200 μm. *P < 0.05, **P < 0.01 vs. day 0.

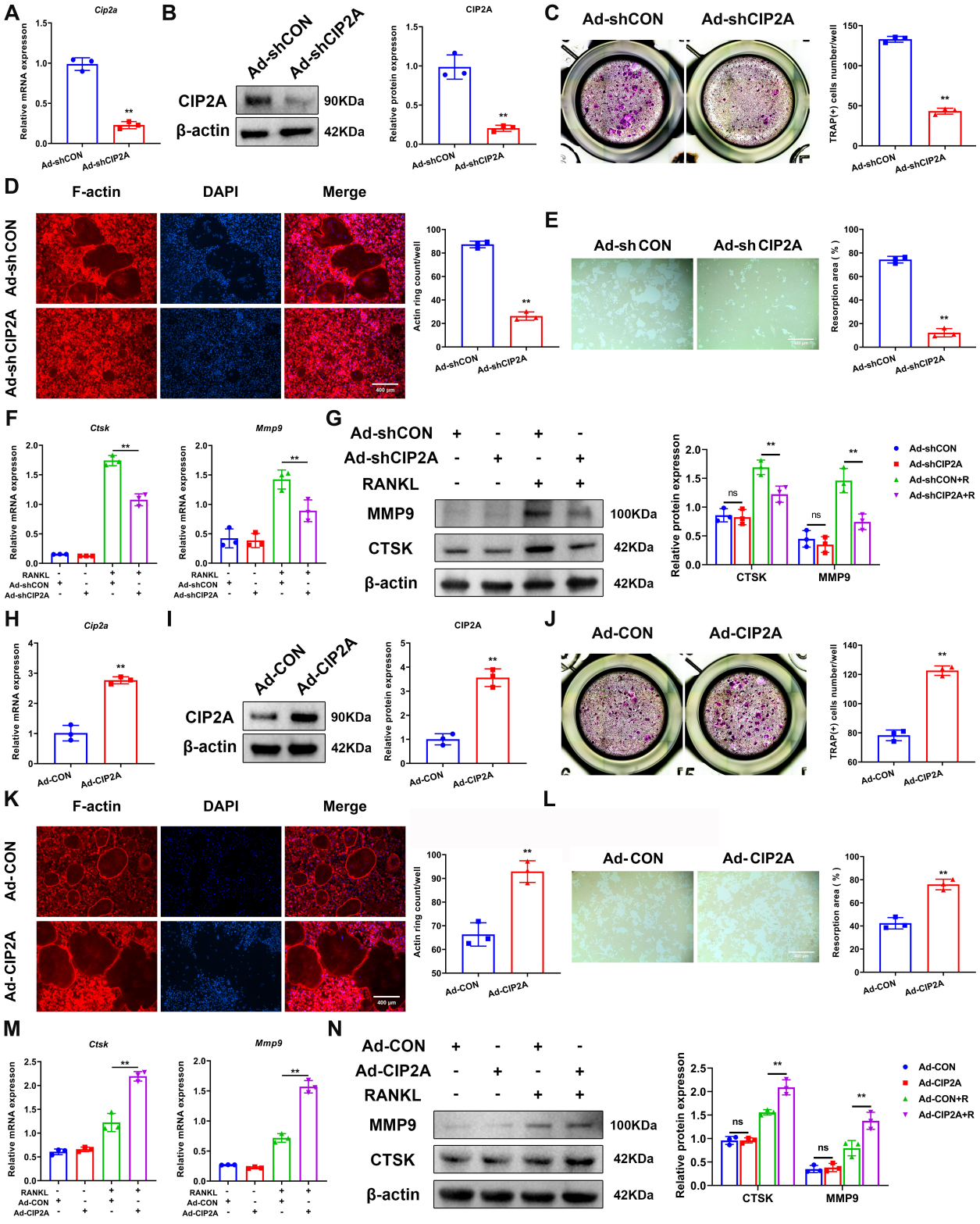


Figure 2

CIP2A promotes osteoclast formation and bone resorption in vitro. (A, B) RT-qPCR and Western blot validation of CIP2A knockdown efficiency in BMMs transduced with Ad-shCIP2A. (C) Representative TRAP-stained osteoclasts and quantification of TRAP-positive multinucleated cells. (D) F-actin ring staining and quantification of ring-bearing osteoclasts. (E) Bone resorption pit assay with resorbed area quantification. (F, G) RT-qPCR and Western blot analysis of CTSK and MMP9 expression following CIP2A knockdown. (H, I) RT-qPCR and Western blot validation of CIP2A overexpression efficiency in BMMs transduced with Ad-CIP2A. (J–N) TRAP staining, F-actin rings, and bone resorption assays under CIP2A overexpression. R, RANKL. Data are presented as mean ± SD. N = 3 independent experiments. Scale bar: 400 μm. *P < 0.05, **P < 0.01 vs. respective control (Ad-shCON or Ad-CON); ns, not significant.

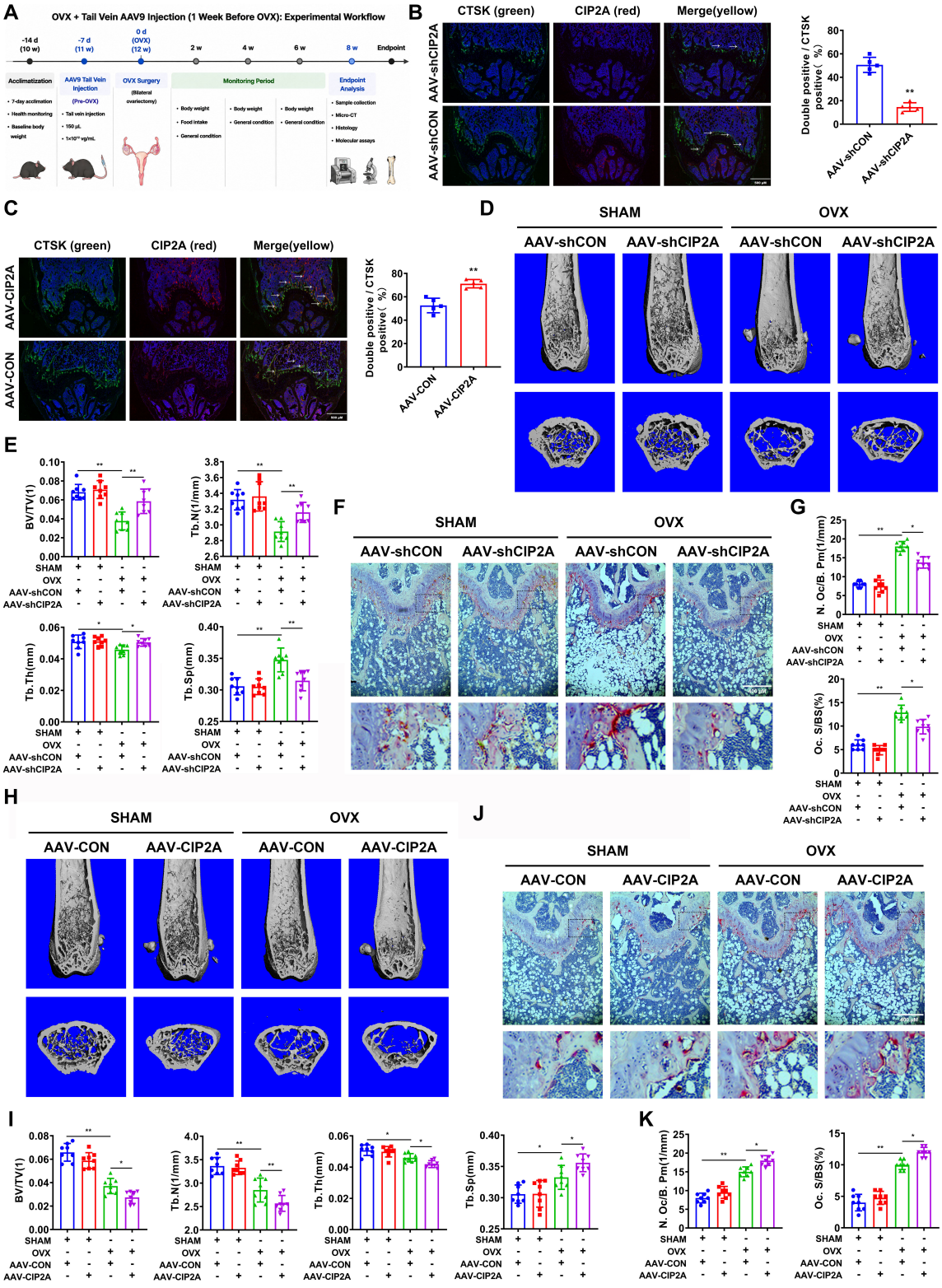


Figure 3

CIP2A modulates OVX-induced bone loss in vivo. (A) Experimental timeline for systemic AAV administration via tail vein for CIP2A overexpression or knockdown in OVX mice. (B, C) Representative immunofluorescence images showing CTSK (green) and CIP2A (red) in distal femoral sections, with merged images indicating co-localization, and quantification of CTSK⁺CIP2A⁺ cells. (D) Micro-CT 3D reconstructions of distal femurs from SHAM+AAV-shCON, SHAM+AAV-shCIP2A, OVX+AAV-shCON, and

OVX+AAV-shCIP2A groups. (E) Quantitative analysis of trabecular parameters: BV/TV, Tb. N, Tb. Th, Tb. Sp. (F) TRAP staining of femoral sections. (G) Histomorphometric quantification of N. Oc/B. Pm and Oc. S/BS. (H-K) Micro-CT and TRAP analyses for OVX mice treated with AAV-CON or AAV-CIP2A. Data are presented as mean ± SD. N = 8 mice/group. Scale bar: 500 μm (B, C), 400 μm (F, J). *P < 0.05, **P < 0.01.

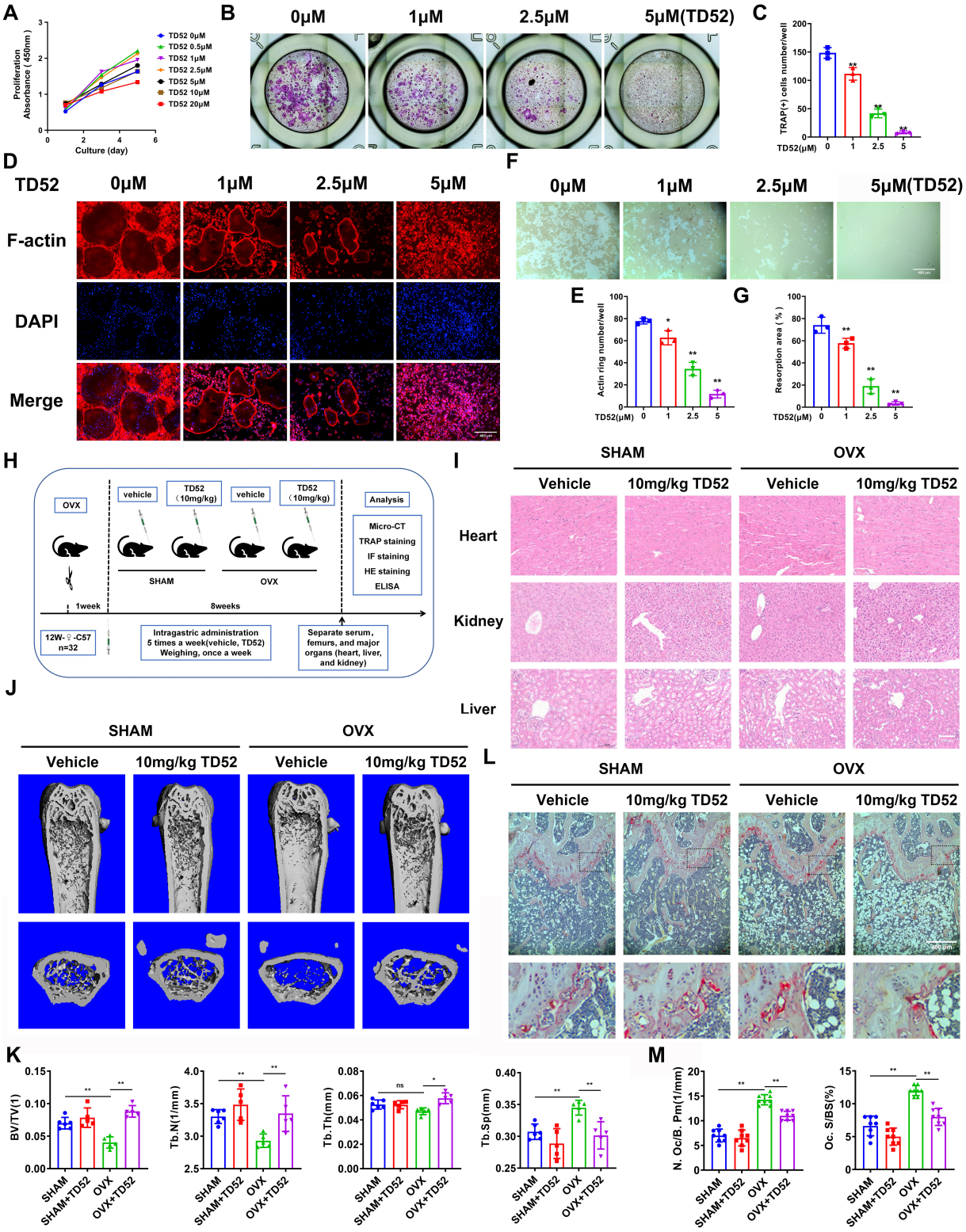


Figure 4

Pharmacological inhibition of CIP2A by TD52 suppresses osteoclastogenesis and bone loss. (A) CCK-8 assay of BMMs viability with TD52 (0–20 μM). (B, C) TRAP staining and quantification of osteoclast formation in the presence of TD52 (0–5 μM). (D, E) F-actin ring staining and quantification. (F, G) Bone resorption pit assay and quantification. (H) Experimental timeline for TD52 administration in OVX mice. (I) H&E staining of heart, liver, and kidney to assess toxicity. (J) Micro-CT reconstructions of distal femurs. (K) Quantitative trabecular parameters. (L) TRAP staining of femoral sections. (M) Histomorphometric quantification of N. Oc/B. Pm and Oc. S/BS. Data are presented as mean ±SD. N = 3 (A-G) or N = 8 mice/group (H-M). Scale bars: 400 μm (D, F, L), 100 μm (I). *$P < 0.05$, **$P < 0.01$ vs. control; ns, not significant.

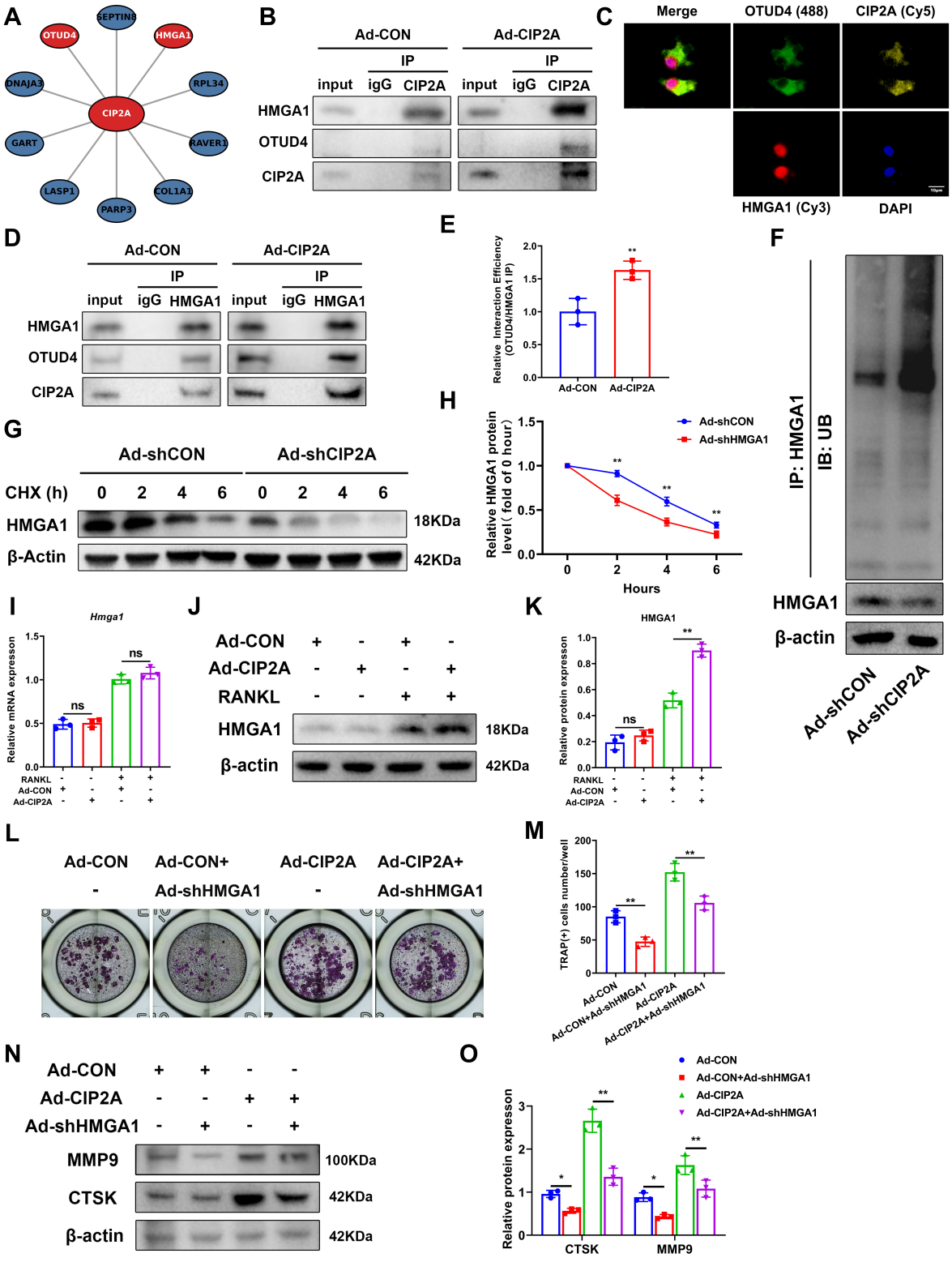


Figure 5

CIP2A recruits OTUD4 to deubiquitinate and stabilize HMGA1. (A) IP–MS identification of top ten CIP2A-interacting proteins. (B) co-IP confirming the interaction of CIP2A with OTUD4 and HMGA1. (C) Immunofluorescence showing CIP2A/OTUD4 cytoplasmic co-localization and HMGA1 nuclear localization. (D, E) Co-IP and quantification showing enhanced OTUD4–HMGA1 interaction upon CIP2A overexpression. (F) Ubiquitination assay showing increased HMGA1 polyubiquitination upon CIP2A

knockdown. (G, H) CHX chase assay and quantification revealing accelerated HMGA1 degradation following CIP2A depletion. (I) RT-qPCR analysis of Hmga1 mRNA after CIP2A overexpression. (J, K) Western blot and quantification of HMGA1 protein levels. (L, M) TRAP staining showing HMGA1 knockdown attenuates CIP2A-induced osteoclast formation. (N, O) Western blot analysis of osteoclast marker proteins. Data are presented as mean ± SD. N = 3 independent experiments. Scale bar: 10 μm. *P < 0.05, **P < 0.01; ns, not significant.

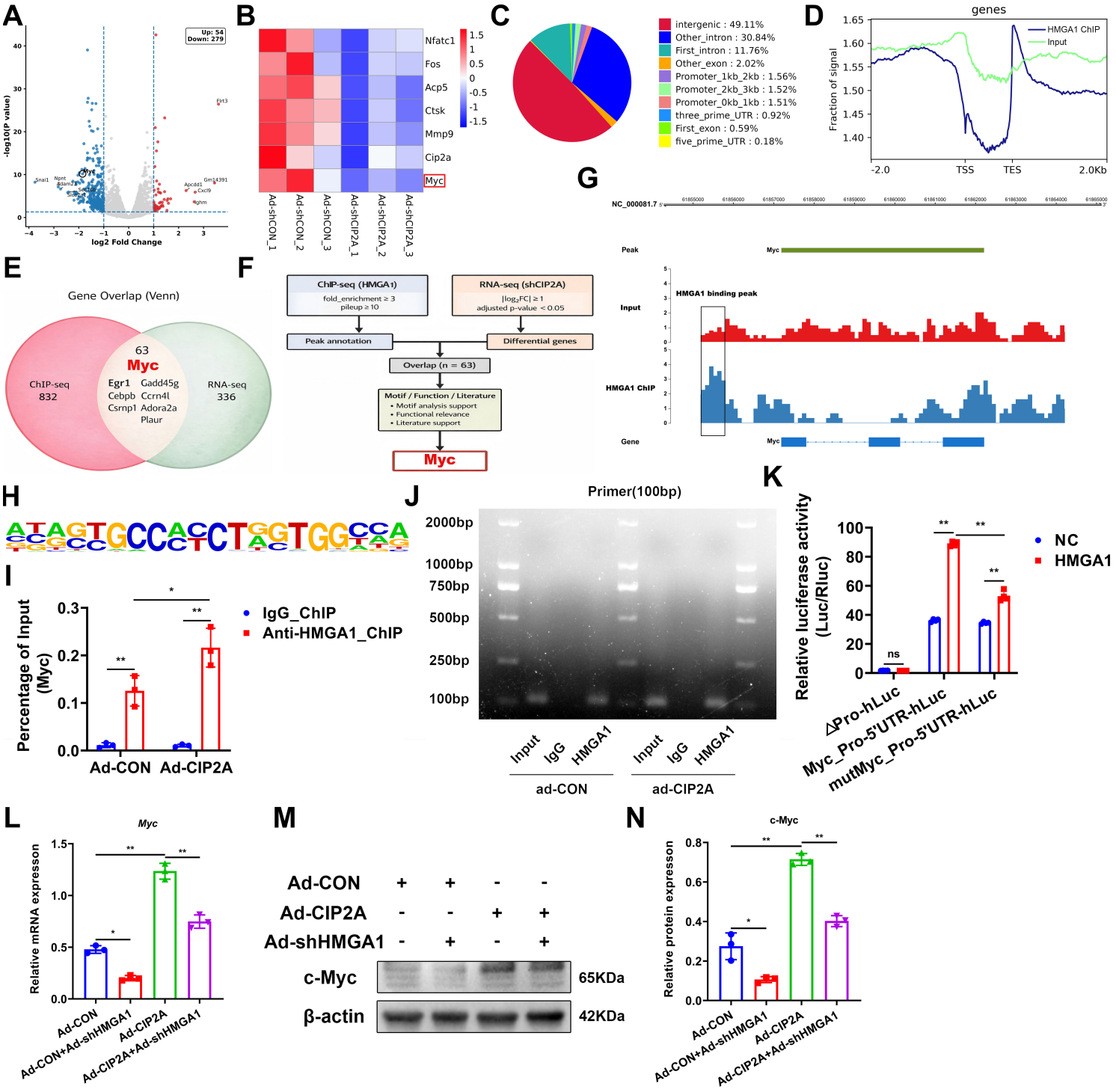


Figure 6

CIP2A–HMGA1 axis promotes c-Myc transcription. (A, B) RNA-seq volcano plot and heatmap showing downregulation of osteoclast-related genes including c-Myc after CIP2A knockdown. (C) Genomic distribution of HMGA1 ChIP-seq peaks. (D) HMGA1 binding profile relative to TSS and TES. (E, F) Venn diagram and gene list intersection of RNA-seq and HMGA1 ChIP-seq datasets, highlighting c-Myc as a candidate target. (G) ChIP-seq signal track displaying HMGA1 binding peaks within the c-Myc genomic locus. (H) Motif analysis showing enrichment of HMGA1 consensus sequence in c-Myc regulatory regions. (I) ChIP-qPCR validation of HMGA1 occupancy at the c-Myc locus with or without CIP2A overexpression. (J) Agarose gel electrophoresis confirming ChIP-qPCR amplicon specificity. (K) Luciferase assay with c-Myc promoter/5'UTR showing HMGA1-dependent transactivation, reduced upon HMGA1 binding site mutation. (L–N) RT-qPCR and Western blot showing CIP2A upregulates c-Myc mRNA and protein; HMGA1 knockdown partially reverses effect. Data are presented as mean ±SD. N = 3 independent experiments. *P < 0.05, **P < 0.01; ns, not significant.

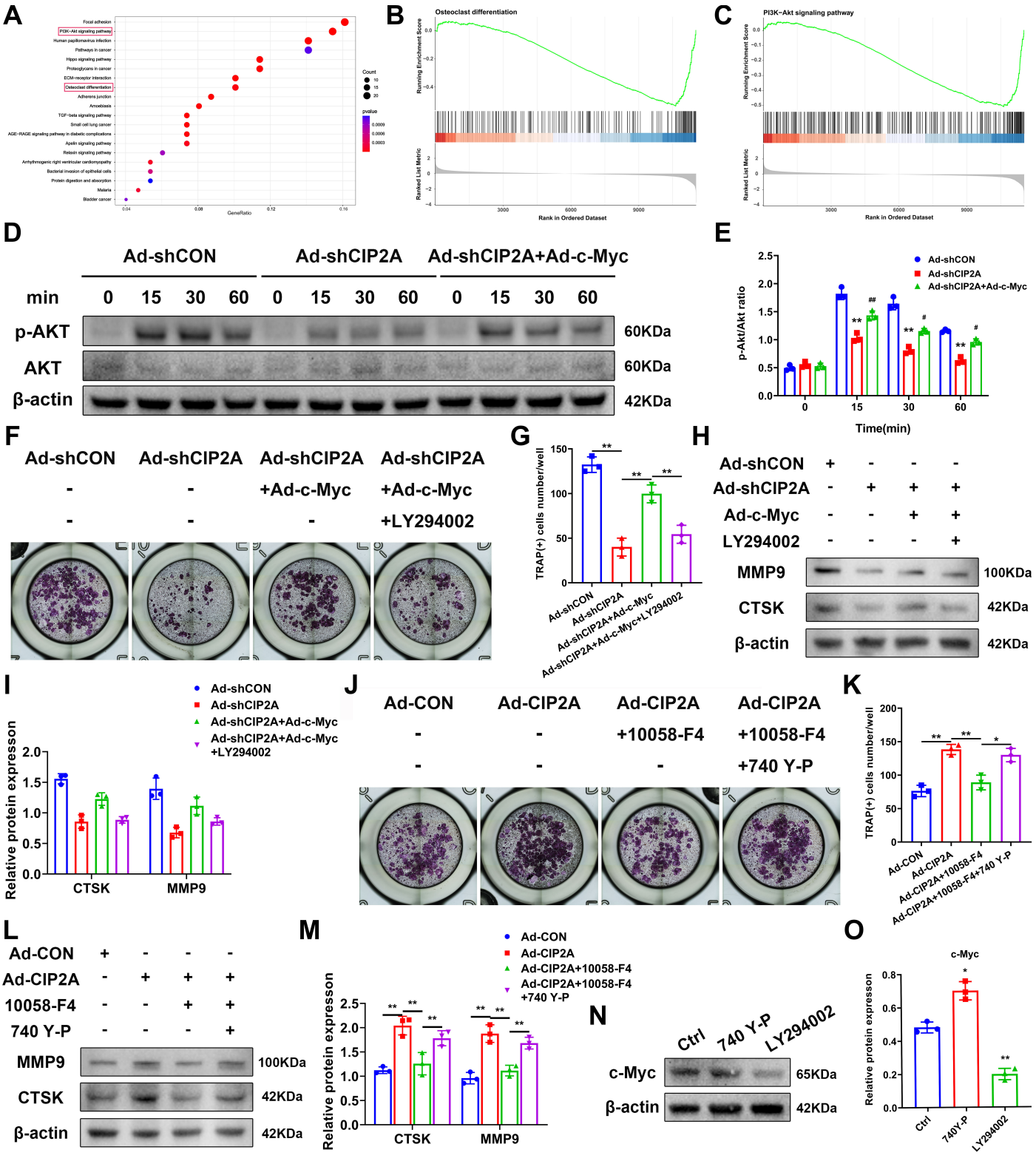


Figure 7

c-Myc–PI3K/AKT feedback loop amplifies CIP2A-driven osteoclastogenesis. (A–C) Pathway enrichment from CIP2A-depleted BMMs RNA-seq showing osteoclast differentiation and PI3K/AKT signaling. (D, E) Western blot and quantification of phosphorylated AKT. CIP2A knockdown reduces RANKL-induced p-AKT; c-Myc overexpression partially restores it. (F, G) TRAP staining showing c-Myc rescues osteoclast formation defect from CIP2A knockdown; PI3K inhibitor LY294002 partially blocks

rescue. (H, I) Western blot analysis of CTSK and MMP9 under the same experimental conditions. (J, K) TRAP staining showing c-Myc inhibitor 10058-F4 suppresses CIP2A overexpression-induced osteoclastogenesis; AKT activator 740 Y-P partially restores it. (L, M) Western blot analysis of CTSK and MMP9 in the same rescue assay. (N, O) Western blot and quantification showing that 740 Y-P upregulates and LY294002 downregulates c-Myc protein. Data are presented as mean ±SD. N = 3 independent experiments. *P < 0.05, **P < 0.01 vs. control; #P < 0.05, ##P < 0.01 vs. Ad-shCIP2A groups.

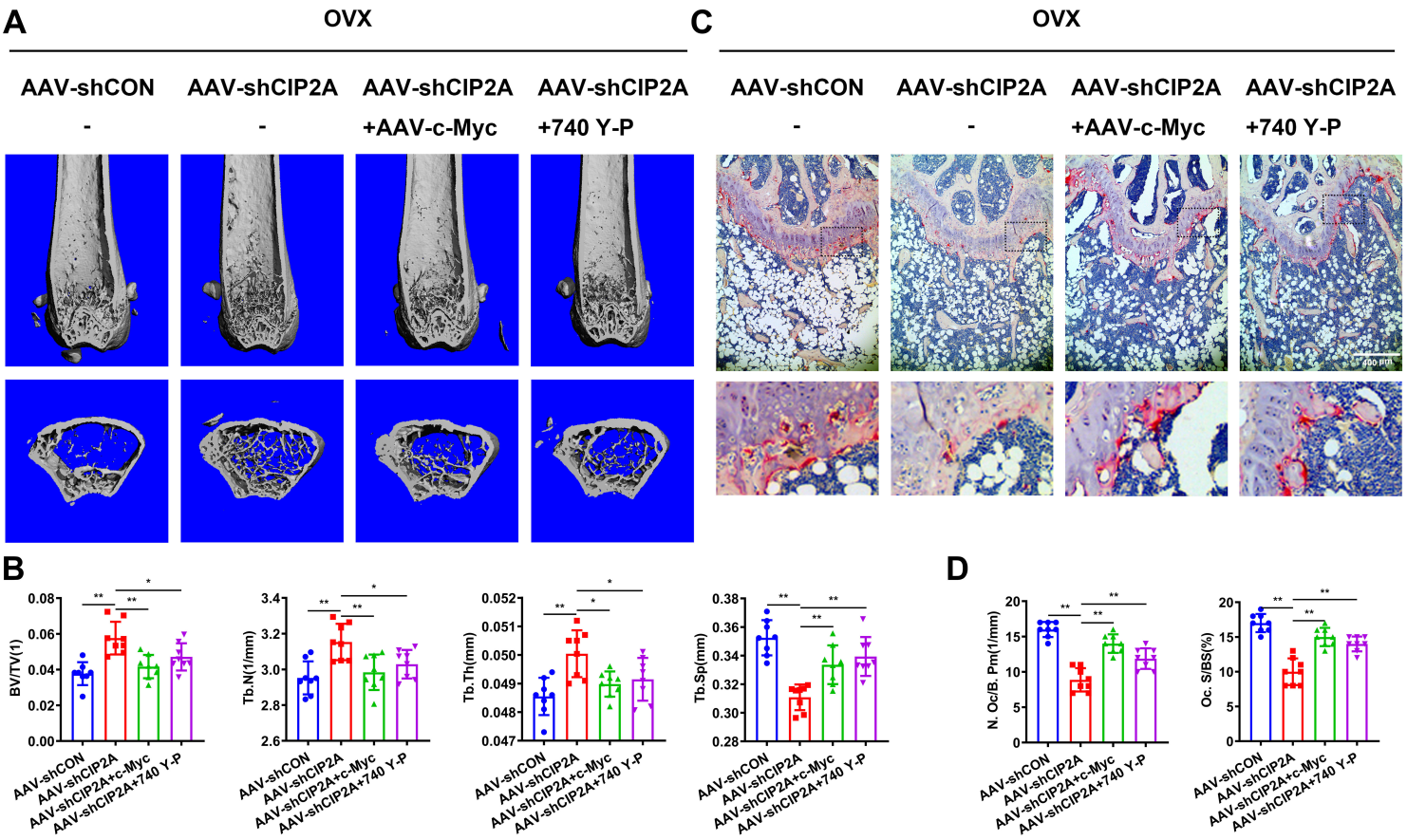


Figure 8

Targeting CIP2A–HMGA1–c-Myc axis alleviates bone loss through the PI3K/AKT pathway in vivo. (A) Micro-CT 3D reconstructions of distal femurs from OVX mice treated with AAV-shCIP2A alone or with c-Myc overexpression or 740 Y-P. (B) Quantitative analysis of trabecular bone parameters (BV/TV, Tb. Th, Tb. N, Tb. Sp). (C) TRAP staining of femoral sections. (D) Histomorphometric quantification of N. Oc/B. Pm and Oc. S/BS. Data are presented as mean ±SD. N = 8 mice/group. Scale bar: 400 μm. *P < 0.05, **P < 0.01.

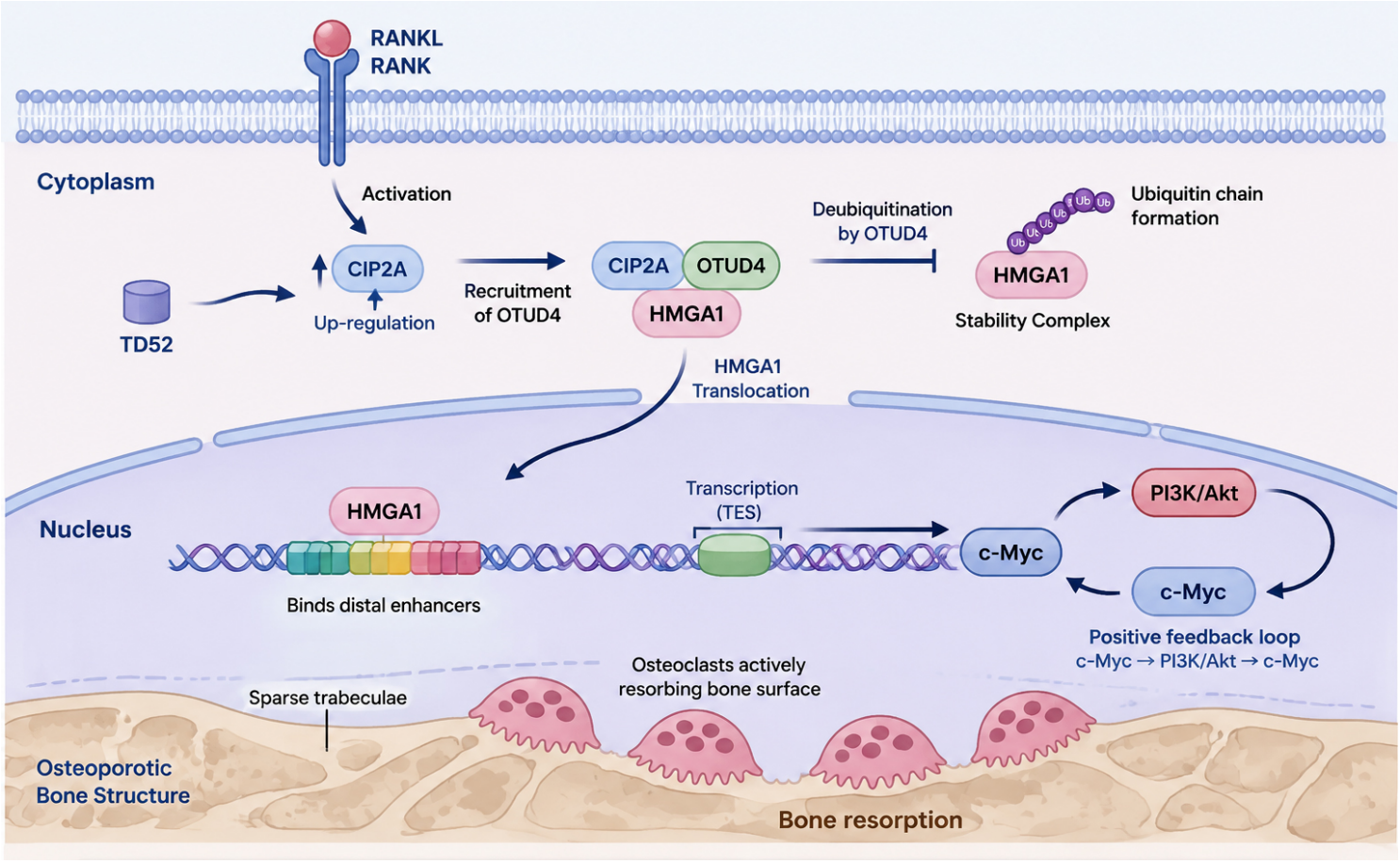


Figure 9

Mechanistic model of CIP2A-mediated osteoclastogenesis and bone resorption.

Supplementary Files

This is a list of supplementary files associated with this preprint. Click to download.

- OriginalimageofWesternblot.docx
- SupplementaryFig.S1andTableS1S5.docx